Impact of Charge Ordering on Magnetic Correlations in Perovskite (Bi, Ca)MnO_3

Wei Bao,[1] J. D. Axe,[1] C. H. Chen,[2] and S-W. Cheong[2]
[1]*Brookhaven National Laboratory, Upton, New York 11973*
[2]*Bell Laboratories, Lucent Technologies, Murray Hill, New Jersey 07974*
(Received 29 May 1996)

Single crystalline $Bi_{1-x}Ca_xMnO_3$ ($0.74 \leq x \leq 0.82$) were studied with neutron scattering, electron diffraction, and bulk magnetic measurement. We discovered dynamic ferromagnetic spin correlations at high temperatures, which are replaced by antiferromagnetic spin fluctuations at a concomitant charge ordering and structural transition. Our results indicate that thermal-activated hopping of the Jahn-Teller active e_g electrons in these insulating materials, nevertheless, induces ferromagnetic interaction through the double-exchange mechanism. It is the ordering of these charges which competes with the double-exchange ferromagnetic metallic state. [S0031-9007(96)02252-1]

PACS numbers: 75.40.Gb, 71.70.Ej, 75.25.+z, 75.30.Et

The relation of double exchange, Jahn-Teller distortion, and charge ordering is one of the central issues in current study on perovskite mixed-valent manganites $T_{1-x}D_xMnO_3$ [1] (T being trivalent ions, e.g., La, Pr, or Nd, and D being divalent ions, e.g., Ca, Sr, Ba, or Pb [2]). In these materials, the mean number of 3D electrons per Mn can be tuned from 4 to 3. Because of strong Hund rule coupling, Mn^{3+} has a high-spin state $t_{2g}^3 e_g^1$ and the e_g level is split by Jahn-Teller distortion. For the Mn^{3+}-end members, the long range order of the elongated MnO_6 octahedra (with d_{z^2}-type orbitals for this kind of Jahn-Teller distortion) stabilizes an insulating antiferromagnetic ground state [3–5]. In doped samples, e_g electron hopping [6] between Mn^{3+} and Mn^{4+} neighbors induces ferromagnetic correlations through the so-called double-exchange mechanism [7]. It is well known that for x larger than a threshold value, a ferromagnetic metallic ground state becomes stable [8,9]. A structural transition to a higher symmetry state also occurs at the threshold [10], which results from the ability of the hopping e_g electrons to destroy the long range coherence of the Jahn-Teller distortion (or d_{z^2}-type orbitals) [4]. Long range order of charges in the $Mn^{4+}(t_{2g}^3)$-rich regime was recently observed with electron diffraction in $La_{1-x}Ca_xMnO_3$ ($x > 0.5$) [11]. A large anomaly in sound velocity was found at the charge ordering temperature. More interestingly, the magnetic susceptibility $\chi(T)$ has a pronounced inflection at the charge ordering temperature, resembling that associated with a conventional long range antiferromagnetic transition [12]. However, thermodynamic measurements suggest that the antiferromagnetic order develops at a lower temperature [11]. In order to clarify and understand the anomalous lattice and magnetic phenomena at charge ordering, microscopic information is crucial, and neutron scattering is the ideal probe for this purpose with its access to static and dynamic correlations of both magnetic and structural degrees of freedom [13].

Single crystals of $La_{1-x}Ca_xMnO_3$ ($x > 0.5$) are not available. However, we have succeeded in growing single crystals of isostructural $Bi_{1-x}Ca_xMnO_3$ in this Mn^{4+}-rich regime. As the following description will show, (Bi,Ca)MnO_3 bears close resemblance to (La,Ca)MnO_3 in the overlapping composition range, attesting to the identical underlying physics. Single crystals of (Bi,Ca)MnO_3, however, allow us to extract much more information with neutron scattering. We found that the charge ordering is accompanied by a structural transition and antiferromagnetic long range order indeed develops at a lower temperature. The most important of our discoveries, however, is that the nature of spin fluctuations changes from *ferromagnetic* to *antiferromagnetic* at the charge ordering transition. These results indicate that, at high temperatures, thermally activated e_g electron hopping in the insulating regime, nevertheless, induces ferromagnetic correlations through the double-exchange mechanism. When e_g electrons with their accompanying Jahn-Teller distortions freeze in static order, the double exchange induced ferromagnetic spin fluctuations are replaced by superexchange antiferromagnetic spin fluctuations.

Single crystals of $Bi_{1-x}Ca_xMnO_3$ were grown using the flux method. The compositions of samples were determined by inductive coupled plasma emission spectroscopy. The weights of samples used in neutron scattering are 25, 127, and 320 mg for $x = 0.74$, 0.76, and 0.82, respectively. Charge ordering was observed with electron diffraction using a JOEL 2000FX transmission electron microscope. Superlattice peaks with wave vector $(\delta, 0, 0)$ in $Pbnm$ notation appear below a charge ordering temperature T_O similar to those in (La,Ca)MnO_3 [11]. $\delta \simeq 0.30$ and 0.22 for $x = 0.74$ and 0.82, respectively. The decreasing δ is consistent with the decreasing numbers of e_g electrons, which are involved in the charge ordering. Figure 1(a) shows the development of the charge superlattice intensity of (0.22,0,0) below $T_O = 210$ K for a $x = 0.82$ sample. Magnetic susceptibility was measured for crystals from the same batches with a Quantum Design SQUID magnetometer. Consistent results were found for different crystals from the same batch. Figure 1(b) shows an example for $x = 0.82$. At high temperatures, the Curie-Weiss law is followed, yielding an effective moment $p = 4.15(2)\mu_B$, which is close to the expected $p = 4.08$ for this

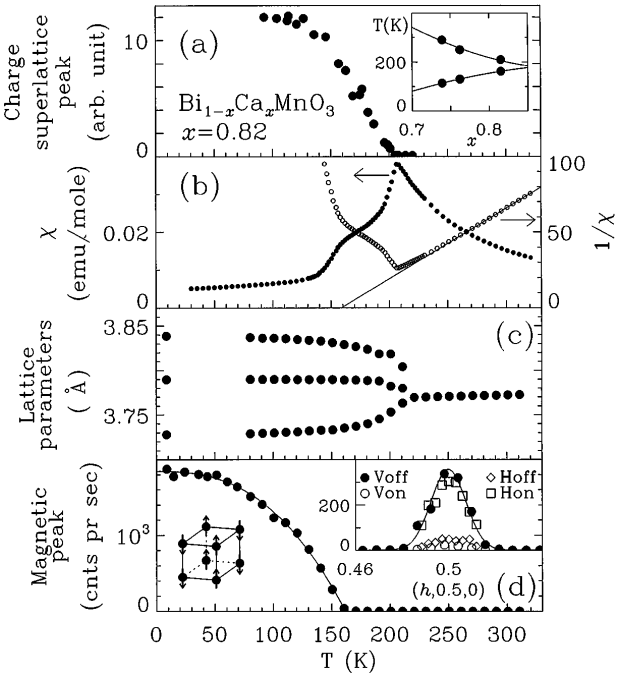

FIG. 1. Temperature dependences of (a) intensity of the charge superlattice peak, (b) magnetic susceptibility χ, (c) pseudocubic lattice parameters, and (d) intensity of magnetic Bragg peak (1/2,1/2,0) for a $x = 0.82$ sample. $1/\chi$ (open circles) is also shown in (b) with scale to the right and the straight line is a fit to the Curie-Weiss law. Polarized neutron scattering of (1/2,1/2,0) is shown in the right inset of (d): solid and open circles are for the flipper turned off (Voff) and on (Von) cases with a magnetic field along (001); diamonds and squares for flipper off (Hoff) and on (Hon) with the magnetic field along the scattering wave vector. The spin structure determined is shown in the left corner of (d). Inset in (a): temperature-composition phase diagram for $Bi_{1-x}Ca_xMnO_3$, showing the charge-structural transition T_O (upper curve) and the Néel temperature T_N (lower curve).

composition. The positive value of the Weiss constant $\Theta = 159(1)$ K reveals the existence of ferromagnetic correlations between Mn spins. The drastic reduction of $\chi(T)$ at the charge ordering temperature T_O is similar to that observed in (La,Ca)MnO_3 [12]. At 160 K, there begins a further reduction in the magnetic susceptibility, whose origin will become clear after the presentation of our neutron scattering results.

Neutron scattering experiments were conducted with triple axis spectrometers at the High Flux Beam Reactor at Brookhaven National Laboratory. Except for polarized neutron scattering, graphite monochromators and analyzers were used. High order contaminations were removed with graphite filters. At room temperature, the selection rules for nuclear Bragg peaks are consistent with space group *Pbnm*. However, the orthorhombic distortion is small. For the purpose of this paper, we use the simpler pseudocubic perovskite unit cell [14]. Figure 1(c) shows the pseudocubic lattice parameters as a function of temperature for a $x = 0.82$ sample. At the charge ordering temperature T_O, there is a structural transition, as evidenced by the splitting of the Bragg peaks. This result is not totally surprising, since each e_g electron carries with it a Jahn-Teller lattice distortion. When e_g electrons order, long range correlations can develop among Jahn-Teller distorted MnO_6 octahedra [4].

In a pioneering powder neutron diffraction study, three types of magnetic structures were reported in the composition range $0.74 \le x \le 0.82$ for $La_{1-x}Ca_xMnO_3$ [3]. We have conducted a thorough search in (hk0) and (hhl) zones of (Bi,Ca)MnO_3 at low temperatures. For all of our samples, magnetic Bragg peaks are found only at *C*-type points $(\frac{2n+1}{2}, \frac{2m+1}{2}, l)$. We distinguished magnetic peaks from structural superlattice peaks not only with temperature dependence, but more conclusively using polarized neutron scattering. Heusler crystals were used both as monochromator and analyzer, and a spin flipper and a graphite filter were placed in the diffracted beam. The inset on the right of Fig. 1(d) shows an example of a (1/2,1/2,0) scan for the $x = 0.82$ sample. By aligning a magnetic field along different directions at the sample position, the magnetic nature of the Bragg peak is proven and the spin direction is determined [15]. In the current case, spin lies along the *c* axis, as found in (La,Ca)MnO_3 for a *C*-type antiferromagnet [3]. The resulting spin structure is shown in the left inset to Fig. 1(d). Possible implications of this magnetic structure for e_g orbital ordering has been discussed by Goodenough [4]. Comparing the magnetic and nuclear Bragg intensities, the staggered magnetic moment at 9 K is determined to be $3.5(2)\mu_B$ per Mn. This corresponds to an average Mn spin $S = 1.8(1)$, and $p = 2\sqrt{S(S+1)} = 4.4(3)$ is in good agreement with that given by susceptibility measurement at high temperatures. The temperature dependence of the order parameter in Fig. 1(d) establishes the Néel temperature $T_N = 160$ K for $x = 0.82$, which coincides with the lower inflection point of $\chi(T)$ in Fig. 1(b). The Néel temperature T_N and the charge-structural transition temperature T_O for various samples are summarized in the inset to Fig. 1(a). This phase diagram parallels that of (La,Ca)MnO_3 [11], pointing to a generic behavior for both systems.

After establishing the phase relation and the magnetic ground state, let us now turn to dynamic spin properties. Figure 2(a) shows spin-wave dispersion along three symmetry directions for $x = 0.82$ measured at 11 K near a magnetic zone center. The spin Hamiltonian which describes Mn spins below charge ordering transition is

$$\mathcal{H} = \sum_{\langle i,j\rangle_{\mathrm{AF}}} J_{\mathrm{AF}} \mathbf{S}_i \cdot \mathbf{S}_j + \sum_{\langle i,j\rangle_{\mathrm{F}}} J_{\mathrm{F}} \mathbf{S}_i \cdot \mathbf{S}_j - g\mu_B H_u \sum_i |S_i^z| ,$$

where J_{AF} and J_{F} are antiferromagnetic and ferromagnetic nearest neighbor interactions [refer to Fig. 1(d)] and H_u is a uniaxial anisotropy field. Each nearest neighbor spin pair is counted only once in the summations. Conventional

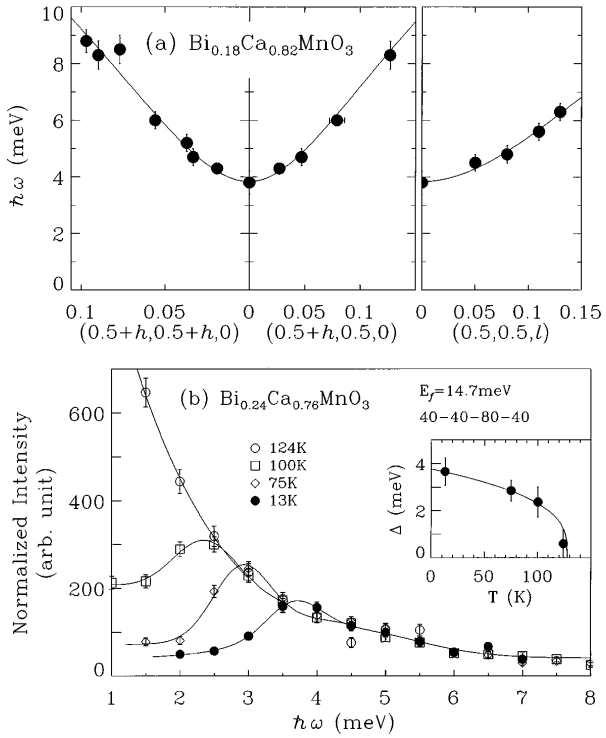

FIG. 2. (a) Spin-wave dispersion along (110), (100), and (001) around the magnetic zone center (1/2,1/2,0), measured at 11 K for $x = 0.82$. The solid curves represent a fit to the spin-wave dispersion relation of Eq. (1). (b) Energy scans at (1/2,1/2,0) for $x = 0.76$ at various temperatures. The energy gap, Δ, of the spin excitations collapses when the Néel $T_N = 130$ K is approached.

spin wave theory yields the dispersion relation [13]

$$\hbar\omega(\mathbf{q}) = \sqrt{[J(0) - J_1(0) + J_1(\mathbf{q}) + g\mu_B H_u]^2 - J(\mathbf{q})^2}\,, \tag{1}$$

where $\mathbf{q} = (hkl)$ is the wave vector from an antiferromagnetic zone center, $J(\mathbf{q}) = 2SJ_{\mathrm{AF}}[\cos(2\pi h) + \cos(2\pi k)]$, and $J_1(\mathbf{q}) = 2SJ_{\mathrm{F}}\cos(2\pi l)$. This dispersion relation accounts well for our data, as indicated by the solid curves in Fig. 2(a). From the fit we derive $SJ_{\mathrm{AF}} = 3.6(1)$ meV, $SJ_{\mathrm{F}} = -1.3(1)$ meV, and $H_u = 4.4(3)$ T. The zone boundary energy at (0,0,1/2) derived using these parameters is 13.8(8) meV for this $T_N = 160$ K bipartite 3D antiferromagnet. Recently, the spin wave dispersion has been measured for ferromagnetic samples [16–18]. A Heisenberg nearest neighbor model describes well the experimental results at low temperatures. The nearest neighbor exchange varies from $SJ = -12.6(5)$ meV at 27 K to $-7.6(3)$ meV at 300 K for $La_{0.7}Sr_{0.3}MnO_3$ [16]; for $La_{0.7}Pb_{0.3}MnO_3$ and $La_{0.77}Ca_{0.33}MnO_3$, the corresponding value at $T \to 0$ is $-8.8(2)$ meV [17] and -11.4 meV [18], respectively. Ferromagnetic double exchange in these samples appears to be stronger than the antiferromagnetic superexchange measured in our sample [19].

There is an energy gap $\Delta = 3.8$ meV in the spin-wave excitations of Fig. 2(a). Compared with $k_B T_N = 13.8$ meV, this is a very large spin gap. Similar spin gaps were also found for $x = 0.74$ and 0.76 samples. A constant $\mathbf{q}$ scan for $x = 0.76$ at (1/2,1/2,0) is shown in Fig. 2(b). This explains the pronounced reduction of $\chi(T)$ below T_N. A similar, but less pronounced, reduction of χ in the case of $La_{1-x}Ca_xMnO_3$ ($x > 0.5$) [11,12] is likely also to be caused by the development of a spin gap below T_N. The softening of the spin gap with elevated temperatures was measured, and the results are shown in Fig. 2(b). We explain the spin gap in our insulating samples with uniaxial anisotropy. This could be a natural consequence of the ordering of the d_{z^2} orbitals. Meanwhile, rapid hopping of d_{z^2} electrons in the metallic phase renders spin space isotropic and no gap in spin excitations is expected for the ferromagnetic manganites. This is indeed what was found experimentally for $La_{0.77}Ca_{0.33}MnO_3$ with neutron scattering [18].

To investigate the anomalous reduction of $\chi(T)$ at the charge-structural transition, we have directly measured dynamic spin correlations with inelastic neutron scattering. Antiferromagnetic spin fluctuations were probed at (1/2,1/2,0) [Fig. 3(b)] and ferromagnetic spin fluctuations near the forward direction [Fig. 3(c)], where magnetic form factor maximizes and structure factor for structural fluctuations diminishes as q^2. As charge order parameter grows below T_O [refer to Fig. 3(a)], *ferromagnetic* spin fluctuations are replaced by *antiferromagnetic* spin fluctuations. This may be better seen in Fig. 3(a), which shows detail temperature variations of both the ferromagnetic response (open circles, measured at $\hbar\omega = 1$ meV and $q = 0.17$ Å^{-1}) and the antiferromagnetic response [solid circles, measured at $\hbar\omega = 1.7$ meV and $\mathbf{q} = (1/2, 1/2, 0)$]. The absence of antiferromagnetic spin correlations above T_O is evidenced by a flat background both in the energy scan and in $\mathbf{q}$ scans [refer to Fig. 3(b)] at (1/2,1/2,0). The lower energy limit of this flat background was pushed down to 0.4 meV with better resolution of cold neutron scattering. There is obviously not any ferromagnetic component in the low temperature magnetic order [see Fig. 1(b)]. This justifies our use of low temperature data as the background for ferromagnetic response in Fig. 3(a), and the inset in 3(c) shows the net ferromagnetic intensity at 215 K by subtracting background measured at 70 K. Therefore our experimental results establish that ferromagnetic interactions exist between spins above T_O and they are replaced by antiferromagnetic interactions when charge orders. This switching of magnetic correlations from a ferromagnetic type to an antiferromagnetic type explains the inflection of $\chi(T)$ at T_O.

A separate antiferromagnetic transition below a charge ordering transition was discovered previously in laminar perovskites $Sr_{2-x}La_xMnO_4$ for $x \sim 0.5$ [20]. This material also has an insulating antiferromagnetic ground state, and the high temperature ferromagnetic susceptibility is interrupted by charge ordering, as in the Mn^{4+}-rich (La,Ca)MnO_3 and (Bi,Ca)MnO_3. Meanwhile,

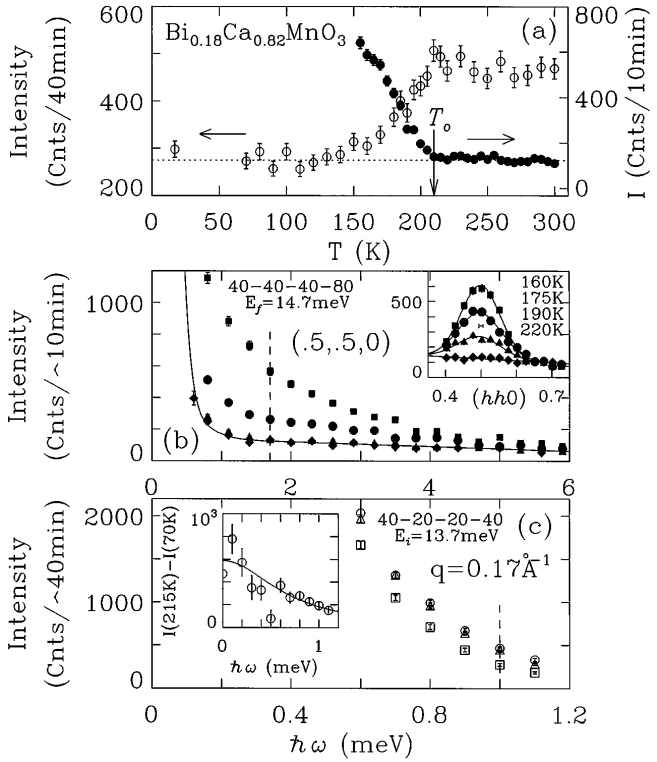

FIG. 3. (a) Temperature dependence of antiferromagnetic response measured at (1/2,1/2,0) and 1.7 meV (solid circles), and ferromagnetic response at $|\mathbf{q}| = 0.17$ Å^{-1} and 1 meV (open circles) [marked with dashed lines in (b) and (c) respectively]. The dotted line indicates background (see text for details). Below the charge ordering transition at $T_O = 210$ K, ferromagnetic response is replaced by antiferromagnetic response. (b) Energy scans at the antiferromagnetic zone center (1/2,1/2,0) at 165 K (squares), 190 K (circles), 220 K (triangles), and 300 K (diamonds). The solid line connects data at 300 K, which are indistinguishable from those at 220 K. Inset shows constant $\hbar\omega = 1.7$ meV scans at temperatures indicated. (c) Energy scans near the forward direction with $|\mathbf{q}| = 0.17$ Å^{-1}, probing ferromagnetic fluctuations, at 70 K (squares), 215 K (circles), and 300 K (triangles). Inset shows 215 K data with background at 70 K subtracted, and the solid line is a Lorentzian.

double-exchange ferromagnetic ground state coincides with metallic conduction both in perovskite manganites for $x \sim 0.3$ [21] and double layered $(La_{0.4}Sr_{0.6})_3Mn_2O_7$ [22]. This suggests that the competition between double exchange and the *ordering* of the Jahn-Teller active e_g electron is the dominant factor in determining the ground state of perovskite and related manganites.

In summary, we have observed directly in the Mn^{4+}-rich (Bi,Ca)MnO_3 a simultaneous charge ordering and structural transition. Above the charge-structural transition temperature T_O, there exist ferromagnetic spin fluctuations, indicative of double exchange induced by the e_g electron hopping. Below T_O, we discover the replacement of the ferromagnetic correlations by antiferromagnetic spin fluctuations, which support the notion that the ferromagnetic double exchange diminishes as charge orders. The antiferromagnetic transitionlike inflection point in $\chi(T)$ at T_O is accounted for by this switch from ferromagnetic spin fluctuations to antiferromagnetic fluctuations. *C*-type long range antiferromagnetic order was found to develop in a separate phase transition at a lower temperature with large uniaxial anisotropy, which open a gap in spin excitations.

It is a pleasure to thank C. Broholm, S. M. Shapiro, G. Shirane, Q. Zhu, H. Y. Hwang, B. Batlogg, A. Zheludev, M. Martin, and G. Y. Xu for discussions and assistance. W. B. acknowledges the Aspen Center for Physics where part of the work was performed. Work at BNL was supported by DOE under Contract No. DE-AC02-76CH00016.

[1] A. J. Millis *et al.,* Phys. Rev. Lett. **74**, 5144 (1995).
[2] J. B. Goodenough and J. M. Longon, in *Landolt-Börnstein, New Series III* (Springer, New York, 1970), Vol. 4, Part a.
[3] E. O. Wollan and W. C. Koehler, Phys. Rev. **100**, 545 (1955).
[4] J. B. Goodenough, Phys. Rev. **100**, 564 (1955).
[5] T. Mizokawa and A. Fujimori, Phys. Rev. B **51**, 12 880 (1995); T. Saitoh *et al., ibid.* **51**, 13 942 (1995).
[6] Hopping of an e_g electron inevitably carries a Jahn-Teller lattice distortion with it. In other words, the charge motion is polaronic. We freely use e_g electron for this Jahn-Teller polaron in this paper.
[7] C. Zener, Phys. Rev. **82**, 403 (1951); P. W. Anderson and H. Hasegawa, *ibid.* **100**, 675 (1955); P.-G. de Gennes, *ibid.* **118**, 141 (1960).
[8] G. H. Jonker and J. H. Van Santen, Physica (Utrecht) **16**, 337 (1950); J. H. Santen and G. H. Jonker, *ibid.* **16**, 599 (1950).
[9] J.-H. Park *et al.,* Phys. Rev. Lett. **76**, 4215 (1996).
[10] G. Matsumoto, J. Phys. Soc. Jpn. **29**, 606 (1970); **29**, 615 (1970).
[11] A. P. Ramirez *et al.,* Phys. Rev. Lett. **76**, 3188 (1996).
[12] P. Schiffer, A. P. Ramirez, W. Bao, and S-W. Cheong, Phys. Rev. Lett. **75**, 3336 (1995).
[13] S. W. Lovesey, *Theory of Neutron Scattering from Condensed Matter* (Clarendon Press, Oxford, 1984).
[14] Detail crystallographic study will be published later.
[15] R. M. Moon, T. Riste, and W. C. Koehler, Phys. Rev. **181**, 920 (1969). Finite counts for horizontal field with flipper off and vertical field with flipper on are due to imperfection of the polarizing instruments.
[16] M. C. Martin *et al.,* Phys. Rev. B **53**, 14 285 (1996).
[17] T. G. Perring *et al.,* Phys. Rev. Lett. **77**, 711 (1996).
[18] J. W. Lynn *et al.,* Phys. Rev. Lett. **76**, 4046 (1996).
[19] K. Hirota *et al.* (to be published). Spin-wave excitations of *A*-type antiferromagnetic $LaMnO_3$ was measured recently. $SJ_F = -3.34(5)$ meV, $SJ_{AF} = 2.42(6)$ meV, and $H_u = 5.3(1)$ T.
[20] W. Bao *et al.,* Solid State Commun. **98**, 55 (1996).
[21] R. M. Kusters *et al.,* Physica (Amsterdam) **155B**, 362 (1989); K. Chahara *et al.,* Appl. Phys. Lett. **63**, 1990 (1993); H. L. Ju *et al.,* Phys. Rev. B **51**, 6143 (1995); A. Urushibara *et al., ibid.* **51**, 14 103 (1995); H. Y. Hwang *et al.,* Phys. Rev. Lett. **75**, 914 (1995).
[22] Y. Moritomo *et al.,* Nature (London) **380**, 141 (1996).